

A glacier-ocean interaction model for tsunami genesis due to iceberg calving

by Wolper, Gao, Lüthi, Heller, Vieli, Jiang, Gaume

SUPPLEMENTARY MATERIAL

Supplementary Note 1: Detailed description of the non-associative Cam-Clay model for ice

The hyperelastic model, yield surface and hardening law are defined in the main text. Here, we more specifically describe the plastic flow and the definition of the deviatoric hardening variable. Concerning the plastic flow rule, let us define $\mathbf{b}^E = \mathbf{F}^E(\mathbf{F}^E)^T$ as the elastic left Cauchy-Green strain tensor, and $\mathbf{C}^P = (\mathbf{F}^P)^T\mathbf{F}^P$ as the plastic right Cauchy-Green strain tensor. Combining this with our multiplicative decomposition of the deformation gradient, $\mathbf{F} = \mathbf{F}^E\mathbf{F}^P$, we have the following properties: $\mathbf{F}^E = \mathbf{F}\mathbf{F}^{-P}$ and $\mathbf{F}^{E^T} = \mathbf{F}^{P-T}\mathbf{F}^T$. We may then rewrite \mathbf{b}^E as $\mathbf{b}^E = \mathbf{F}\mathbf{F}^{-P}\mathbf{F}^{P-T}\mathbf{F}^T$. Taking the inverse of \mathbf{C}^P as $\mathbf{C}^{-P} = \mathbf{F}^{-P}\mathbf{F}^{P-T}$ reveals a more useful expression: $\mathbf{b}^E = \mathbf{F}\mathbf{C}^{-P}\mathbf{F}^T$. Combining these, we can then consider the evolution of \mathbf{b}^E :

$$\frac{D\mathbf{b}^E}{Dt} = \frac{D\mathbf{F}}{Dt}\mathbf{C}^{-P}\mathbf{F}^T + \mathbf{F}\mathbf{C}^{-P}\frac{D\mathbf{F}^T}{Dt} + \mathbf{F}\frac{D\mathbf{C}^{-P}}{Dt}\mathbf{F}^T. \quad (\text{S.1})$$

We follow the operator splitting scheme proposed by Simo (1988) in which we first integrate the first two terms while ignoring the third (noting that only the third term depends on plastic flow). This can be thought of as taking a "trial" elastic step from $\mathbf{b}^{E,n}$ to an intermediate state, $\mathbf{b}^{E,tr}$; in practice, we achieve this through evolving \mathbf{F} from t^n to t^{n+1} while ignoring plasticity. We then use this as an initial value condition for solving the remaining integration. We further simplify this by defining the material Lie derivative, $\mathcal{L}_v\mathbf{b}^E$, to be this remaining term, giving the following:

$$\frac{D\mathbf{b}^E}{Dt} = \mathbf{F}\frac{D\mathbf{C}^{-P}}{Dt}\mathbf{F}^T = \mathcal{L}_v\mathbf{b}^E = -2\gamma\mathbf{G}\mathbf{b}^E. \quad (\text{S.2})$$

Here, γ is a scalar related to the magnitude of plastic dissipation and \mathbf{G} is the direction of plastic flow; in this context, \mathbf{G} can be thought of as the direction we must project along to return material points back to feasible stress states, while γ is related to the distance. Inspired by the principle of maximum plastic dissipation, Gaume et al. (2018) chose an associative flow rule which projects stress states orthogonally to the yield surface and uses $\mathbf{G} = \frac{\partial y}{\partial \boldsymbol{\tau}}$ where y is the yield surface and $\boldsymbol{\tau}$ is the Kirchoff stress. However, recall that this approach is inadequate for a non-porous material such as ice. As such, we choose a non-associative flow rule which instead projects orthogonally to the hydrostatic axis using $\mathbf{G} = \text{dev}(\frac{\partial y}{\partial \boldsymbol{\tau}})$.

We discretize Eq. (S.2) using the recent backward Euler approach of Wolper et al. (2019):

$$\mathbf{b}^{E,n+1} - \mathbf{b}^{E,tr} = -2\delta\gamma\mathbf{G}(\mathbf{b}^{E,n+1})\mathbf{b}^{E,n+1} \quad (\text{S.3})$$

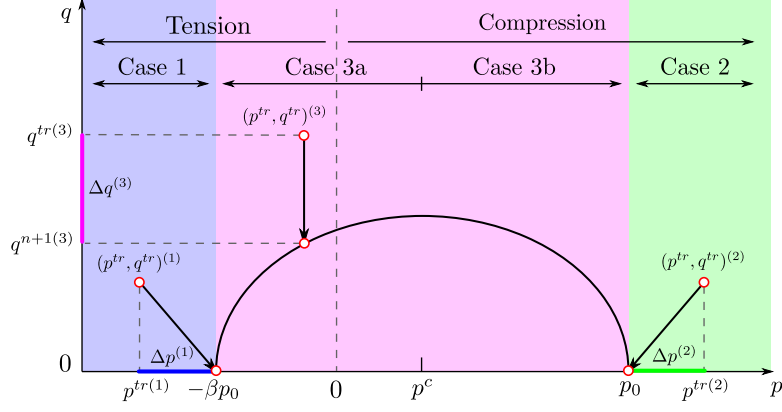
where $\delta\gamma := \gamma\Delta t$ in our discretization. We further expand this expression by decomposing \mathbf{b}^E into its deviatoric and dilational components:

$$\mathbf{b}^E = \text{dev}(\mathbf{b}^{E,n+1}) + \frac{1}{d}\text{tr}(\mathbf{b}^{E,n+1})\mathbf{I}. \quad (\text{S.4})$$

Combining this split with Eq. (S.3) of this supplement and Eq. (4) of the paper (definition of \mathbf{s}) and taking the deviatoric part of each side reveals that for relatively stiff materials, \mathbf{s}^{tr} and \mathbf{s}^{n+1} are vectors in the same direction (this is leveraged in Simo (1988) as well):

$$\frac{\mathbf{s}^{tr}}{\|\mathbf{s}^{tr}\|} = \frac{\mathbf{s}^{n+1}}{\|\mathbf{s}^{n+1}\|}. \quad (\text{S.5})$$

With this theory in place we may now outline our return mapping approach. The return mapping entails first computing the trial elastic step for each particle to get \mathbf{F}^E for each particle. Then, we use the definition of $p := -\frac{1}{d}\text{tr}(\boldsymbol{\tau}) = -J^E\Psi\kappa'(J^E)$ to compute p^{tr} for each particle (the intermediate pressure after the first step of the operator splitting scheme). Based on the trial stress state, we may determine which of the three cases each particle lies in. In Fig. 1 we illustrate these three cases by color:



Supplementary Figure 1: **Cohesive Cam Clay yield surface in the $p - q$ space illustrating our new q -based hardening approach.** Red points represent the $p - q$ state of a given particle before and after return mapping in each case. Note that in cases 1 and 2, return mapping simply projects the trial stress to the ellipsoid tips. These tips are analytically well defined, and as such we can simply use the quantities $\Delta p^{(1)}$ and $\Delta p^{(2)}$ for hardening in cases 1 and 2, respectively. However, for case 3, we apply non-associative return mapping and, as such, lack any change in p that could be used to compute the new consolidation pressure. To avoid this issue, our new q -hardening approach proposes to instead use $\Delta q^{(3)}$ to update p_0 for particles undergoing case 3 stresses.

- Case 1: $p^{tr} < -\beta p_0$ and $p^{n+1} = -\beta p_0$
- Case 2: $p^{tr} > p_0$ and $p^{n+1} = p_0$
- Case 3: $-\beta p_0 < p^{tr} < p_0$ and $p^{n+1} = p^{tr}$

Notice that in cases 1 and 2 the trial pressure is entirely outside of the range of feasible pressures outlined by the CCC yield surface. As such, we directly project these stress states to the corresponding ellipsoid tips. Furthermore, because $q^{n+1} = 0$ in these cases, we have a closed form expression (from our definition of p) for $J^{E,n+1}$ and directly know that p^{n+1} is either $-\beta p_0$ or p_0 in cases 1 and 2, respectively:

$$J^{E,n+1} = \sqrt{\frac{-2p^{n+1}}{\kappa} + 1}. \quad (\text{S.6})$$

Using $J^{E,n+1}$ we can easily reconstruct the projected elastic deformation gradient: $\mathbf{F}^{E,n+1} = \mathbf{U}(J^{E,n+1})^{\frac{1}{d}}\mathbf{I}\mathbf{V}^T$ where \mathbf{U} and \mathbf{V} are from $\mathbf{F}^{E,tr} = \mathbf{U}\Sigma\mathbf{V}^T$. However, in case 3 projection we have a non-zero q^{n+1} , and this requires computing $\mathbf{b}^{E,n+1}$. We accomplish this by separately computing the deviatoric and dilational components as in Eq. (S.4). First, $\text{dev}(\mathbf{b}^{E,n+1})$ can be found using the yield surface equation with the assumptions our non-associative flow rule provides us: $p^{n+1} = p^{tr}$ (in case 3). Specifically, we first combine the definition of $q := \sqrt{\frac{6-d}{2}}\|\mathbf{s}\|$ with Eq. (5) of the paper (yield surface definition) to compute $\|\mathbf{s}^{n+1}\|$:

$$\|\mathbf{s}^{n+1}\| = M \sqrt{\frac{2(p^{tr} + \beta p_0)(p^{tr} - p_0)}{(d-6)(1+2\beta)}} \quad (\text{S.7})$$

We use $\|\mathbf{s}^{n+1}\|$ and Eq. (S.5) to compute \mathbf{s}^{n+1} , and then, using Eq. (4) of the paper (definition of \mathbf{s}), we have an expression for $\text{dev}(\mathbf{b}^{E,n+1})$:

$$\text{dev}(\mathbf{b}^{E,n+1}) = \frac{\mathbf{s}^{n+1}}{\mu J^{\frac{-2}{d}}} \quad (\text{S.8})$$

As for the dilational component, we get this easily from taking the trace of both sides of Eq. (S.5):

$$\text{tr}(\mathbf{b}^{E,n+1}) = \text{tr}(\mathbf{b}^{E,tr}) \quad (\text{S.9})$$

Finally, we construct the case 3 updated elastic deformation through $\mathbf{F}^{E,n+1} = \mathbf{U}\sqrt{\mathbf{b}^{E,n+1}}\mathbf{V}^T$.

The final step in our return mapping approach is to update the hardening/softening of each particle. Intuitively this can be thought of as absorbing the influence of \mathbf{F}^P (and any associated plastic dissipation) into a hardening variable, α , that is used to compute the material consolidation pressure (recall that p_0 is computed using Eq. (6) of the paper). Changes in p_0 change the size of the yield surface, and as such, particles either harden or soften based on these updates; note that this material softening is what allows the ice to fracture in our model. Fortunately, it is trivial to compute hardening updates for cases 1 and 2, and in fact, changes in α for cases 1 and 2 correspond exactly to changes in $\log(J^P)$. We simply take the determinant of both sides of $\mathbf{F}^{E,tr} \mathbf{F}^{P,tr} = \mathbf{F}^{E,n+1} \mathbf{F}^{P,n+1}$ to formulate a direct update for α (in cases 1 and 2):

$$\alpha^{n+1} = \alpha^n + \log\left(\frac{J^{E,tr}}{J^{E,n+1}}\right) \quad (\text{S.10})$$

We use p^{tr} and p^{n+1} with Eq. (S.6) to compute this update. We illustrate this in Fig. 1: for case 1 and 2 hardening we use the change in p to compute hardening; however, case 3 poses a problem: there is no change in p for our non-associative flow rule. Wolper et al. (2019) successfully perform case 3 hardening using a fairly complex geometric intersection approach that has little physical grounding. As such, we propose to instead focus on the change in q for case 3.

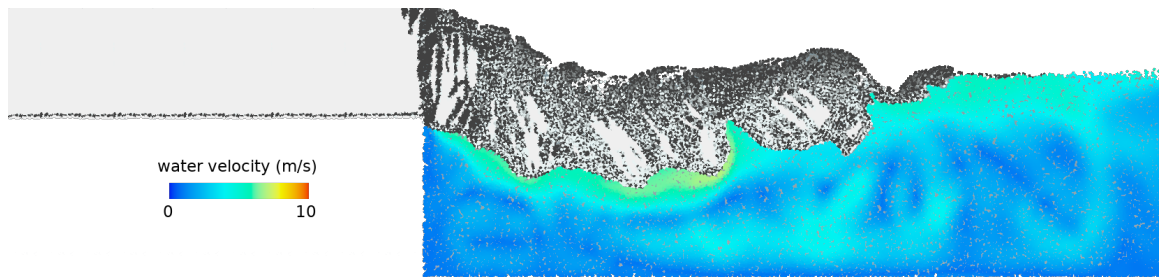
We design our q -hardening approach based on the observation that p and J have a quadratic relationship: $p = C(J^2 - 1)$ where C is a constant. Inspired by this, we design the quantity ζ to have a similar quadratic relationship to q . Specifically, we let $\|\text{dev}(\mathbf{b})\| = \zeta^2 - 1$ which in turn, combined with the definition of q , gives:

$$\zeta^* = \sqrt{\frac{q^* J^{tr \frac{2}{d}}}{\mu \sqrt{\frac{6-d}{2}}} + 1} \quad (\text{S.11})$$

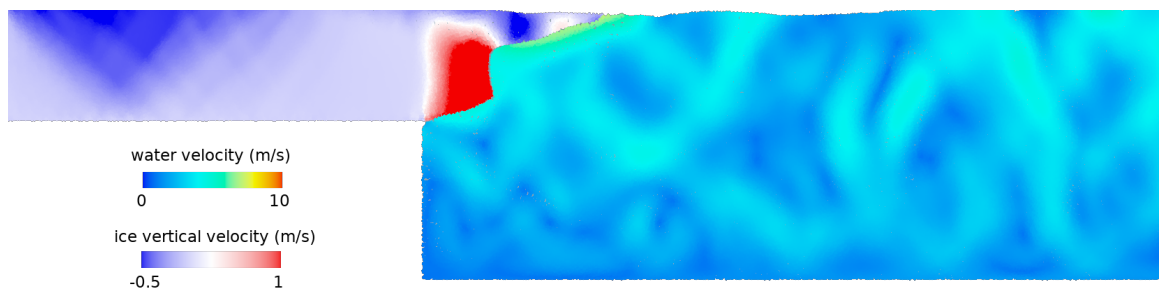
where $* \in \{tr, n+1\}$. This allows us to use a similar hardening update to Eq. (S.10), but instead of J^{tr} and J^{n+1} , we compare ζ^{tr} and ζ^{n+1} . However, this has one further complication: $\log(\frac{\zeta^{tr}}{\zeta^{n+1}})$ is always positive (this is clear from Fig. 1). As such, in order to correctly model both hardening and softening in case 3 we check which side of the yield surface center p^{tr} is on to determine whether the particle should harden or soften ($p^c = (1 - \beta)p_0/2$). More specifically, our case 3 hardening rule is as follows:

$$\alpha^{n+1} = \begin{cases} \alpha^n - \log\left(\frac{\zeta^{tr}}{\zeta^{n+1}}\right) & p^{tr} \geq p^c \text{ (hardening)} \\ \alpha^n + \log\left(\frac{\zeta^{tr}}{\zeta^{n+1}}\right) & p^{tr} < p^c \text{ (softening)} \end{cases}$$

At last, this allows us to model both hardening and softening in case 3 while obviating the need for any non-physical geometric solutions as in Wolper et al. (2019).



Supplementary Figure 2: **Calving characteristics for low ice tensile strength.** The following parameters were used: $D/H_i = 0.2$, $\beta p_0 = 10$ kPa, $M = 1.4$ and $N = 5$. Failed ice particles are colored in grey. In this case with low tensile strength, multiple small icebergs are released.



Supplementary Figure 3: **Calving characteristics for very low ice tensile strength and friction.** The following parameters were used: $D/H_i = 0.8$, $\beta p_0 = 1$ kPa, $M = 0.13$ and $N = 5$. In this case with low tensile strength and low friction, the glacier flows in a ductile manner. The red area has a positive velocity meaning that the ice is lifted up due to buoyancy.

Supplementary References

- Gaume, J., T. Gast, J. Teran, A. van Herwijnen, and C. Jiang, 2018: Dynamic anticrack propagation in snow. *Nature Communications*, **9**(1), 3047.
- Simo, J. C., 1988: A framework for finite strain elastoplasticity based on maximum plastic dissipation and the multiplicative decomposition: Part i. continuum formulation. *Computer Methods in Applied Mechanics and Engineering*, **66**(2), 199–219.
- Wolper, J., Y. Fang, M. Li, J. Lu, M. Gao, and C. Jiang, 2019: CD-MPM: Continuum damage material point methods for dynamic fracture animation. *ACM Trans. Graph.*, **38**(4).